1 **In silico screen identifies a new *Toxoplasma gondii* mitochondrial ribosomal**
2 **protein essential for mitochondrial translation**
3
4
5 Alice Lacombe[1], Andrew E. Maclean[1], Jana Ovciarikova[1], Julie Tottey[1,2] and Lilach
6 Sheiner[1]*
7
8
9 Author affiliation:
10
11 [1] Wellcome Centre for Integrative Parasitology, University of Glasgow, 120 University
12 Place Glasgow G12 8TA, UK
13 [2] UMR 1282 ISP, INRA-Université François Rabelais de Tours, Nouzilly, France.
14
15
16 *Corresponding author:
17 Lilach Sheiner, lilach.sheiner@glasgow.ac.uk ,ORCID ID - 0000-0001-5909-2307
18
19
20
21 Keywords:
22 Toxoplasma ; mitochondria ; translation ; ribosome ; screen
23
24

Summary

Apicomplexan parasites cause diseases such as malaria and toxoplasmosis. The apicomplexan mitochondrion shows striking differences from common model organisms, including in fundamental processes such as mitochondrial translation. Despite evidence that mitochondrial translation is essential for parasites survival, it is largely understudied. Progress has been restricted by the absence of functional assays to detect apicomplexan mitochondrial translation, a lack of knowledge of proteins involved in the process and the inability to identify and detect mitoribosomes.

Using mRNA expression patterns, 279 candidate mitochondrial housekeeping components were identified in *Toxoplasma*. 11 were validated, including the mitoribosomal small subunit protein 35 (*Tg*mS35). *TgmS35* tagging enabled the detection of a macromolecular complex corresponding to the mitoribosomal small subunit for the first time in apicomplexans. A new analytical pipeline detected defects in mitochondrial translation upon *Tg*mS35 depletion, while other mitochondrial functions remain unaffected. Our work lays a foundation for the study of apicomplexan mitochondrial translation.

Abbreviated summary

The apicomplexan mitochondrion is divergent and essential yet poorly studied. Mitochondrial translation is predicted to utilize ribosomes assembled from fragmented rRNA but this was never shown. Knowing the mitochondrial protein content is critical for these studies. We identified 11 new mitochondrial proteins via *in-silico* searches. Tagging and depletion of a mitoribosomal small subunit protein enabled the first detection of a macromolecular ribosomal complex, and provided proof of principle for our new mitochondrial translation analytic pipeline.

Introduction

Mitochondria are organelles of central importance to eukaryotic cells, providing key nutrients and metabolites. Mitochondria are present in virtually all eukaryotic cells, excluding a rare case of secondary loss (Karnkowska et al., 2016; Karnkowska and Hampl, 2016). The recent interest in evolutionary cell biology has resulted in an increasing appreciation of the diverse features of mitochondria found in divergent organisms, which includes differences in fundamental pathways such as protein translation (e.g. Ramrath et al., 2018). However, most of our knowledge of mitochondrial biology is still based on studies in organisms that represent a small proportion of the range of eukaryotic diversity, thus limiting our understanding. One of the challenges to the study of mitochondrial biology in diverse organisms is the lack of tools to identify and functionally characterise genes encoding species or phylum specific mitochondrial proteins.

Apicomplexa is a phylum of parasitic protists with high impact on human health globally, which includes the malaria causing *Plasmodium* spp and the causative agent of toxoplasmosis, *Toxoplasma gondii*. Apicomplexans represent one of the lineages whose mitochondrial biology is understudied despite numerous pieces of evidence of its essential role in parasite biology. The apicomplexan mitochondrion hosts an array of essential metabolic pathways (van Dooren et al., 2006; Sheiner et al., 2013). In addition, its central role in parasite survival is highlighted in recent screens for genes important for fitness in *T. gondii* (Sidik et al., 2016) and *Plasmodium berghei* (Bushell et al., 2017). Both screens showed that high numbers of genes encoding mitochondrial proteins are important for fitness. Finally, mitochondrial pathways are the focus of drug discovery studies (e.g. Srivastava et al., 1997; Nilsen et al., 2013; Phillips et al., 2015), including evidence that mitochondrially encoded proteins are promising targets for the development of antimalarials that may circumvent the emergence of drug resistance (Goodman et al., 2016; Klug et al., 2016). It is therefore ever more pressing to expand the studies of mitochondrial biology in these organisms. In this work, we focus on *T. gondii*, a tractable model organism for the phylum.

Some features of the apicomplexan mitochondrion that are divergent compared to the more widely studied yeast, mammal and plant mitochondria have been described. For example, apicomplexans have a single mitochondrion that often spans the entire parasite cell periphery (Seeber et al., 1998; Kudryashev et al., 2010; Ovciarikova et al.,2017). Likewise, the apicomplexan mitochondrion has an extremely reduced genome, with size ranging from 6-11 Kb (Vaidya et al, 1989; Hikosaka et al., 2013), encoding only three proteins. These three proteins are subunits of complexes of the mitochondrial electron transport chain (mETC): cytochrome *b* subunit (Cytb) of complex III, and cytochrome *c* oxidase subunits I and III (CoxI and III) of complex IV (Lin et al., 2011; Feagin, 1992, Suplick et al., 1988, Vaidya et al., 1989, Cinar et al., 2015; He et al. 2014, Ogedengbe et al., 2014). The respiratory chain in apicomplexan differs from more commonly studied mitochondria by lacking complex I (NADH dehydrogenase) and have

100   further different composition of complexes IV (Seidi et al., 2018) and complex V
101   (Salunke et al., 2018; Huet et al., 2018); Finally, mitochondrial translation, which is
102   considered a fundamental pathway in eukaryotes, appears to be highly unusual. For
103   example, *Plasmodium* ribosomal RNAs display a high degree of fragmentation (Feagin
104   et al., 2012; Hillebrand et al., 2018) and it is unclear how these small RNA fragments
105   come together to form a ribosome. Moreover, while evidence for the mitochondrial
106   import of ribosomal and ribosome assembly proteins start to emerge (Ke et al., 2018;
107   Gupta et al., 2018a; Gupta et al; 2018b), no evidence that they form a macromolecular-
108   complex that could correspond to a ribosome has been produced. Nevertheless, it is
109   expected that mitochondrial translation is active in apicomplexans. This was inferred
110   from a combination of findings: a study in *P. falciparum* asexual stages showed that an
111   active mETC is essential for replenishing ubiquinone, which is needed to accept
112   electrons from the parasite dihydroorotate dehydrogenase (DHODH) enzyme (Painter et
113   al., 2007). This was shown by an elegant cross species complementation with the yeast
114   DHODH which uses fumarate as the electron acceptor (Painter et al., 2007). In addition,
115   it was found that resistance to atovaquone, which is an antimalarial drug that inhibits the
116   parasites mETC, is acquired through mutations within the mitochondrial gene encoding
117   the Cytb subunit (Siregar et al., 2008). Together these observations highlight an active
118   mitochondrial translation system essential for the mETC to function and thus for parasite
119   survival. Further support is provided indirectly, by the observed import of tRNAs into the
120   mitochondrion of *T. gondii* and *P. falciparum* (Esseiva et al., 2004, Pino et al., 2010;
121   Sharma and Sharma, 2015). Finally, it was recently shown that a putative mitochondrial
122   ribosomal protein is essential for *P. falciparum* growth, and that its depletion results in
123   mitochondrial biogenesis defects (Ke et al., 2018). However, the observed phenotype
124   upon gene depletion could not be rescued via complementation with yeast DHODH (Ke
125   et al., 2018), leaving some uncertainties about the link between mitochondrial translation
126   and mETC function in *Plasmodium* asexual stages. No direct evidence for this link, or
127   indeed for active mitochondrial translation, is available in *T. gondii*.
128
129   Here we report the identification of 11 new *T. gondii* mitochondrial proteins identified in a
130   bioinformatics screen that is based on patterns of mRNA co-expression. Among those
131   we identified an apicomplexan mitochondrial ribosomal protein with homology to small
132   subunit 35, whose function is not studied also in other systems including human. We
133   demonstrate that *Tg*mS35 is part of a macromolecular-complex, providing the first
134   evidence for the assembly of a mitochondrial ribosome in an apicomplexan parasite. We
135   show that *Tg*mS35 is important for parasite growth, and that shortly after *Tg*mS35
136   depletion a mitochondrial complex, whose subunits are encoded in the mitochondrial
137   genome, shows decreased activity, while other complexes remain active. These
138   observations provide evidence that *T. gondii* mitochondrial translation is active and that it
139   depends on *Tg*mS35.
140
141

142
143

4

Results:

mRNA expression correlation identifies 279 T. gondii genes encoding potential mitochondrial proteins

It was previously shown that patterns of mRNA expression during the *T. gondii* tachyzoite cell cycle have functional predictive power (Behnke et al., 2010; Sheiner et al., 2011). We reasoned that mRNA expression patterns could be used to predict genes encoding components of mitochondrial housekeeping pathways such as translation. At the time of performing this search, the apicomplexan mitochondrial protein import pathway had the most components predicted, we therefore assembled a group of 14 *T. gondii* homologs of these components based on the prediction made in (van Dooren et al., 2006)(Table S1.1, top table). We expected that other parasite mitochondrial housekeeping proteins would share mRNA expression patterns with the genes within this group of search-baits. Accordingly, we queried the microarray data generated from synchronised *T. gondii* tachyzoites with these 14 baits (Behnke et al., 2010). Three genes (*TGME49_274090/260850/251780*) did not show cyclical expression pattern during the cell cycle, therefore we proceeded with the remaining 11 (Table S1.1). We queried the microarray data for mRNAs whose pattern of expression correlates with that of each of these 11 baits. This search identified 279 genes (Figure 1A, Table S1.2, column B).

Our search criteria were such that each bait was used to query for similar but not identical mRNA expression pattern, namely a search with a given bait does not identify itself. Despite this restriction, the overall resulting dataset includes 10 of the 11 baits used for the searches (TableS1.1, column E), meaning that queries with some baits identified the other baits, providing validation for this approach. Moreover, another four genes encoding protein import components that were not used in the bait list (since they were not predicted at the time the search was performed) are also found in this dataset (TableS1.1, bottom table). Additionally, genes encoding mitochondrial proteins that function in other known (metabolic and physiological) pathways that are not expected to co-express with the mitochondrial protein import encoding genes are indeed underrepresented in the resulting dataset (Figure 1B, TableS1.3, columns I-R), validating this approach's specificity. We observed that 28.3% are predicted to poses a mitochondrial targeting signal with probability score of >0.5 (Figure 1C). We further observed that 56% of the identified genes are predicted to be important for fitness (scores >-6.8 and <-2 in the whole genome CRISPR screen (Sidik et al., 2016)) (Figure 1D, Table S1.3, Column E) compared to 40% predicted to contribute to parasite fitness in the whole genome screen study (Sidik et al., 2016), or 24.824% (2,875 of total 8,637 genes) if running the above score criteria in ToxoDB. Enrichment of genes important for fitness is in line with enrichment in mitochondrial genes, given that they are highly represented in fitness screens (Sidik et al., 2016; Bushell et al., 2017). In contrast, only 39% of the 279 are unique to apicomplexan (Table S1.3, column C) compared to 42.3% (4,899 of total 8,637 genes) in the whole genome, which is only a minor difference.

5

188

Among 15 genes selected from the 279-gene dataset, 11 encode mitochondrial proteins

191

As a proof of principle, we chose 10 genes encoding hypothetical proteins to assess their localisation (Table 1). We primarily used endogenous gene tagging via single homologous recombination to introduce an epitope tag fusion at the protein c-terminal end (Huynh and Carruthers, 2009; Sheiner et al., 2011). Where endogenous tagging was unsuccessful we assessed the localisation via expression of the tagged cDNA from a heterologous promoter. Among the 8 genes for which we obtained detectable signal (Table 1), 7 were mitochondrial (Figure 2A).

199

To sharpen our focus on understudied mitochondrial housekeeping pathways such as mitochondrial translation, we added another filter to our search: we postulated that *Cryptosporidium* spp, that are the only known species among the apicomplexans that lost their mitochondrial genome, likely lost their mitochondrial translation pathway, that is otherwise conserved among other apicomplexans. We queried the datasets for genes that do not have orthologs in any of the three genomes available for *Cryptosporidium* spp, but that do have orthologs in the genome of *Plasmodium falciparum* 3D7. This search identified 43 genes (Table S1.2, column C). In support of an enrichment of translation components in this dataset, we found 5 of the 35 predicted mitochondrial ribosomal proteins (Gupta et al., 2014) in the 43-gene dataset, while none of them is found in 5 lists of 43 randomly chosen genes (Table S1.3, column U). We attempted to localise five genes from this focused dataset chosen at random, and four localised to the mitochondrion (Figure 2B).

213

Transient expression of CAS9 results in mitochondrial morphology defects

215

Having a group of 11 new mitochondrial proteins to study, we wanted to examine whether transiently expressed CRISPR/Cas9 strategy could be used to provide a rapid read-out assay to detect protein's involvement in mitochondrial biogenesis. We hypothesised that abnormal changes in mitochondrial morphology upon gene disruption may be an indicator for a defect in mitochondrial biogenesis. We picked three of the new mitochondrial proteins at random (encoded by *TGME49_263680/214790* and *226280*). For each gene, we co-expressed FLAG-tagged Cas9 (Sidik et al., 2014) along with a targeting single guide RNA (sgRNA)(TableS2). As control, we expressed the Cas9-FLAG alone or with sgRNA for the non-essential SAG1 (*TGME49_233460*) gene for which we do not expect any mitochondrial phenotype upon gene disruption (SAG1sgRNA). At 48 hours post co-transfection, mitochondria were imaged using immunofluorescence and morphologies were analysed (Figure 3A). We observed elevated mitochondrial abnormalities in all conditions tested except the untreated parasites. While a trend of higher abundance of mitochondrial abnormalities was observed for *TGME49_214790*, the data showed no significant difference from the Cas9-only and Cas9+SAG1sgRNA controls (Figure 3A, B). These data suggest that

6

232   transient expression of Cas9 results in mitochondrial morphological abnormalities,
233   excluding this strategy as a reliable tool for rapid identification of genes involved in
234   mitochondrial biogenesis.
235
236   **TGME49_203620 *encodes a ribosomal protein crucial for parasite fitness***
237
238   Due to the complication encountered in analysing mitochondrial biogenesis defects in
239   parasites transiently expressing Cas9, we proceeded with functional analysis using
240   stable genetic manipulation. As a means to explore the role of mitochondrial translation
241   in *T. gondii* survival, we chose to focus on a gene encoding a ribosomal protein. One of
242   the genes found in our screen, *TGME49_203620*, while annotated as hypothetical
243   protein in ToxoDB.org, is a putative homolog of the mitochondrial small subunit 35
244   (mS35) (Gupta et al., 2014; Greber and Ban, 2016). To provide support for this
245   prediction we tested the gel migration patterns of endogenously triple-HA tagged
246   *TGME49_203620*. While *TGME49_203620*'s protein product migrates around 38 KDa
247   under denaturing conditions (Figure 4A), around the predicted size of the part of the
248   protein that is conserved among apicomplexans (Figure S1), it migrates with a high
249   molecular weight (>1000 KDa) complex, when separated under native conditions using
250   blue-native PAGE (Figure 4B). The migration under native conditions could well
251   correspond to the mitochondrial ribosomal small subunit complex. We therefore named
252   *TGME49_203620*, *Tg*m*S35*.
253
254   We generated a *Tg*m*S35* conditional knock down line by replacing its native promoter
255   with an anhydrotetracycline (ATc) repressible promoter. This manipulation was
256   performed as previously described (Sheiner et al., 2011), however with the modification
257   whereby CRISPR/Cas9 was utilised to enhance integration of the promoter replacement
258   cassette (scheme Figure 4C). We named this line *rTgmS35-3xHA*. Inducible promoter
259   integration was confirmed by PCR (Figure 4D) and ATc induced down-regulation was
260   confirmed by qPCR and by western blot using the triple HA tag (Figure 4E-F). We
261   monitored parasite growth by plaque assay which revealed a severe growth defect in
262   response to *Tg*m*S35* depletion, however small plaques revealed that parasites can still
263   grow slowly (Figure 4G). Finally, immunofluorescence analysis detected mitochondrial
264   morphological abnormalities upon *Tg*m*S35* depletion (Figure 4H-I). Together, these
265   results are consistent with *Tg*m*S35* being a mitochondrial ribosomal subunit important
266   for parasite fitness and mitochondrial biogenesis. Using the same genetic manipulation
267   strategy, we generated conditional mutants for two additional genes among the 11 newly
268   identified mitochondrial protein encoding genes and showed that both are important for
269   parasite growth (Figure S2).
270
271   ***A new protocol for evaluation of mitochondrial translation shows that* Tg*mS35 is***
272   ***essential for this pathway***
273
274   In yeast, mS35 is found at the critical point of mRNA entry into the ribosome (Desai et
275   al., 2017). We hypothesised that depletion of *Tg*m*S35* should result in a mitochondrial

7

276 translation defect, however the field lacks an assay to directly monitor mitochondrial
277 translation in *T. gondii*. We therefore monitored the assembly and activity of the
278 respiratory chain complex IV, which is directly dependent on the mitochondrial
279 translation of CoxI and III, and compared it to the assembly and activity of complex V,
280 which is not dependent on mitochondrial translation of its subunits. Using an enriched
281 mitochondrial fraction, obtained from parasites lysed through nitrogen cavitations, we
282 performed high resolution clear-native PAGE followed by an in-gel complex IV and V
283 enzymatic assays, at different time points after *Tg*m*S35* depletion (Figure 5A, B). We
284 found a decrease of complex IV activity at 48 hours and loss of the activity at 96 hours
285 after *Tg*m*S35* depletion. In contrast, the activity of complex V is unchanged at 48 hours
286 and is only decreased at the 96-hour time point indicating an indirect defect (Figure 5A,
287 B). The band observed for complex IV enzymatic activity migrates at a size consistent
288 with a previous report (Seidi et al., 2018). To further confirm its identity as complex IV we
289 performed mass spectrometry analysis of this band which confirmed the complex identity
290 (Table S3).
291
292 In contrast to complex IV, western blot analysis of a native gel from the 96-hour time
293 point showed that the protein import complex, translocon of the outer membrane (TOM),
294 migrates at the same size as the untreated line (Figure 5C). This data suggests that
295 TOM complex, whose components are not encoded in the mitochondrial genome,
296 continues to assemble. To provide further support for TOM complex assembly, we
297 measured protein import into the mitochondrion. A Myc tagged DHFR fused to the
298 mitochondrial targeting signal of HSP60 (Hsp60$_L$-mDHFR-cMyc (van Dooren et al.,
299 2016)) was transiently transfected into the parasites at different time points after
300 *Tg*m*S35* depletion. Upon entry into the mitochondrion, the mitochondrial targeting signal
301 is cleaved off, generating a smaller sized protein which can be visualised by western
302 blot. Upon an import defect, cleavage no longer takes place (van Dooren et al., 2016).
303 We calculated the ratio of signal intensities between the cytosolic un-cleaved protein and
304 the mitochondrial cleaved protein in each condition. We did not observe any significant
305 protein import defect upon *Tg*m*S35* depletion, including at the 96-hour time point (Figure
306 5D). Taken together, these observations suggest that *Tg*m*S35* depletion results in a
307 defect in the assembly and activity specifically of a mitochondrial respiratory complex
308 whose subunits are thought to be encoded in the mitochondrial genome.
309
310
311

Discussion

Research in recent years has expanded our understanding of mitochondrial diversity across the eukaryotes. However, there is still a reliance on a handful of models, such as yeast and mammals or such as plants, when studying basic mitochondrial functions. Focusing on these canonical mitochondria gives a skewed view of mitochondrial function and composition. One of the reasons for this focus is the lack of well-developed, tractable, model organisms outside these key groups. Despite key advances in recent years in studying microbial eukaryotes, there is still a lack of datasets and tools for studying mitochondrial biology in non-model groups. Apicomplexa, which contain the medically important *Plasmodium* and *Toxoplasma* parasites, is such a group where the mitochondria are understudied. The herein described work provides crucial advances by generating proof of principal for the functional prediction of mRNA expression patterns and by establishing an analytical pipeline to identify mitochondrial translation defects.

Co-expression patterns predict new mitochondrial proteins while also providing functional insight about the resulting candidates

To fully understand and explore mitochondrial functions it is necessary to create an inventory of mitochondrial proteins. To date only 88 *Toxoplasma* mitochondrial proteins have been experimentally validated (summarised in (Mallo et al., 2018)). Establishing the proteome through organelle isolation has been a challenge to the apicomplexan field partially due to the association between the mitochondrion and the apicoplast (Kobayashi et al., 2007; Nishi et al., 2008; and our unpublished data). While methods that may resolve this complication are being explored (Hata et al., 2018), other strategies that bypass the reliance on organelle isolation are being utilised. Recent biotin-proximity tagging approaches have made a big step forward (Seidi et al., 2018). However, the resulting dataset covers mainly matrix proteins. Moreover, the number of 421 proposed mitochondrial proteins identified is predicted to be markedly smaller than the total number of mitochondrial proteins estimated through comparison to other species (Salvato et al., 2014; Smith and Robinson, 2018; Panigrahi et al., 2009). Here we demonstrated the power of mRNA expression pattern in *T. gondii* to identify novel mitochondrial components, and thus to expand the repertoire of known mitochondrial proteins. Moreover, a limitation of strategies aimed to create inventories, is that the resulting datasets do not provide functional insights. We provide evidence that the expression-based prediction provides functional insights, as our chosen group of baits enriched for proteins involved in mitochondrial housekeeping. In this, our finding joins previous work in showing that mRNA expression patterns in *T. gondii* are powerful predictive tool for genes in shared functional groups. Behnke et al, who generated the mRNA expression data used for this study, showed that genes known to be involved in the same pathways (e.g. nuclear genome maintenance, microneme adhesins, rhoptry effectors) share mutual expression pattern (Behnke et al., 2010). Likewise, this strategy was used to predict proteins involved in host cell invasion (Huynh and Carruthers, 2016). Moreover, the opposite is also true, when the group of baits is not composed of proteins

9

356 that take part in the same functional pathway, the resulting dataset contains proteins
357 from different functional pathways as we showed for apicoplast proteins (Sheiner et al.,
358 2011). Only 4 of the 11 new mitochondrial proteins identified here are predicted in the
359 Seidi et al., dataset of 421 genes (Table 1). It is possible that the dataset generated here
360 has higher representation of proteins from non-matrix mitochondrial sub compartments
361 (A potential example is TGME49_240270, which is not predicted to have a mitochondrial
362 targeting signal (Table 1)), or of genes encoding non-abundant proteins that may be
363 missed by proteomics analyses (e.g. TGME49_240780, TGME49_201830 and
364 TGME49_312680 (Table 1)).

365

366 Our study focused on mRNAs that co-express with homologs of the mitochondrial
367 protein import machinery components, some of which were recently validated
368 experimentally (van Dooren et al., 2016). In the same study the authors identified new
369 components of these import complexes that were not included in our bait list (van
370 Dooren et al., 2016). The presence of three of these five new import components in our
371 279-gene dataset (Table S1.1, bottom table) lends support to the power of this strategy
372 to identify mitochondrial protein import components, especially considering none of them
373 are found in five lists of randomly chosen 279 genes (Table S1.4, columns B-M). This
374 observation raises the possibility that some other genes in the dataset may take part in
375 protein import. A previous study showed that at least one of the mitochondrial protein
376 translocation complexes has comparable size to other organisms (van Dooren et al.,
377 2016), while homologs of many components known in other organisms are missing in *T.*
378 *gondii* (van Dooren et al., 2016), suggesting that currently unknown components are part
379 of this machinery and that they may be parasite specific. The 109 apicomplexan unique
380 genes in our dataset (Table S1.3, column C) provide candidates for those missing
381 pieces. Another pathway whose components may co-express with protein import
382 components is mitochondrial tRNA import (Esseiva et al., 2004; Pino et al., 2010;
383 Sharma and Sharma, 2015), as in some organisms these two pathways are linked
384 (Seidman et al., 2012; Tschopp et al 2011). Mitochondrial tRNA import is likely essential
385 for mitochondrial translation, for which components are enriched in the 43-gene dataset,
386 proposing these 43 genes as candidate for component of this pathway.

387

388 Localisation of proteins encoded by 13 candidates from the 279-gene dataset, for which
389 a signal was detected by immunofluorescence, identified 11 new *T. gondii* mitochondrial
390 proteins, expanding the group of validated mitochondrial proteins by 11%. Sequence
391 analysis of the 11 proteins demonstrate that our search strategy provides some
392 improvement from the available mitochondrial targeting prediction algorithms, as either
393 two or three of the new mitochondrial proteins are not predicted to target the
394 mitochondrion in two different algorithms (Table 1). These finding highlight the limitation
395 of relying on localisation prediction algorithms for the prediction of apicomplexan
396 mitochondrial proteins. A similar observation was reported in the biotin proximity study
397 (Seidi et al., 2018). This may be one of the reasons for the observation that more than
398 70% of the 279 proteins have low score (under 0.5) for the prediction of mitochondrial
399 targeting when using the MitoProt II algorithm (https://ihg.gsf.de/ihg/mitoprot.html)

400   (Claros and Vincens., 1996). Another reason for this observation is that many of the non-
401   matrix proteins in the dataset utilise other targeting signals. For example, any
402   mitochondrial proteins among the 50 in the dataset that have predicted transmembrane
403   domains (Table S1.3, column F) likely enters the mitochondrion independently of a
404   mitochondrial targeting signal.

405

406   **Mitochondrial morphology captured by immunofluorescence is linked to**
407   **mitochondrial functional defects in *Toxoplasma***

408

409   In model organisms, mitochondrial morphology and function are tightly linked. In support
410   of this also being the case in *Toxoplasma,* recent studies reported rapid mitochondrial
411   remodelling in respond to drastic changes in the growth environments (Ovciarikova et
412   al., 2017; Charvat and Arrizabalaga, 2016). Likewise, the morphological defect observed
413   here upon *Tg*mS35 depletion provides additional support. For this reason, we hoped to
414   use mitochondrial morphological changes as a preliminary indicator for mitochondrial
415   functional defects. However, we found that transient expression of the Cas9
416   endonuclease in *T. gondii* induces mitochondrial morphology defects. This observation
417   should be considered when analysing mitochondrial phenotypes under these conditions.

418

419   **Observation of the mitochondrial ribosome and characterisation of a new**
420   **ribosomal component demonstrate the crucial role of mitochondrial translation in**
421   ***T. gondii***

422

423   A recent structure of the mitochondrial ribosome of *Trypanosoma brucei* showed an
424   evolutionary shift towards a higher ribosome protein content rather than the RNA heavy
425   complexes of mammalian ribosomes (Ramrath et al., 2018). These findings from *T.*
426   *brucei* illustrates the importance of studying basic cellular components in a diverse array
427   of models, however, this is not possible without detecting mitochondrial ribosomes and
428   validating mitochondrial ribosomal proteins. Among the 11 genes we localised here, 4
429   are predicted to be ribosomal subunits. One of those, *TGME49_203620*, while annotated
430   in some databases as hypothetical, shows homology to the mitochondrial small
431   ribosomal subunit 35, mS35, and was therefore renamed *Tg*mS35. Blue-native
432   separation of endogenously tagged *Tg*m*S35* resolved it as a part of a macro-molecular
433   complex, with a size potentially corresponding to the small mitochondrial ribosomal
434   subunit complex. This is the first direct evidence that, despite the apicomplexan
435   fragmented mitochondrial rRNA (Barbrok et al., 2010), the apicomplexan mitochondrial
436   ribosomes are assembled into stable complexes. This is a major step forward in the
437   study of apicomplexan ribosomes which are not well studied and whose composition is
438   not known. While our observation suggests that macro-molecules containing
439   mitochondrial ribosomal proteins form a stable complex, the question of how they
440   assemble and are held together structurally remains open. A recent study identified
441   novel RNA binding proteins in the apicomplexan mitochondrion and proposed the
442   hypothesis that they may participate in ribosome assembly (Hillibrand et al., 2018). The

11

443   tagged ribosomes we generated here can be used in the future to try tackling the
444   question of mitochondrial ribosome structure and function in *T. gondii*.

445

446   **A new protocol to follow mitochondrial translation in *T. gondii***

447

448   The lack of a direct assay to detect mitochondrial translation in Apicomplexa is a major
449   obstacle to study this important pathway. In a recent study, a *P. falciparum* mitochondrial
450   ribosomal protein, the large subunit 13 (which per the new notation (Greber and Ban.,
451   2016) can be named PfuL13m) was characterised (Ke et al., 2018). Like *Tg*mS35, the
452   study found that PfuL13m depletion mutant displayed a growth defect. The authors
453   showed decreased activity of respiratory complex III, whose Cytb subunit is
454   mitochondrially encoded, as a read-out for translation (Ke et al., 2018). However, the
455   inability to rescue the growth defect using an mETC bypass route available for the
456   *Plasmodium* asexual stages (Ke et al., 2018), complicates the analysis of phenotype
457   specificity. Here we generated an analytic pipeline that, while still indirect, provides
458   specificity for a translation dependent outcome. We show that conditional depletion of
459   *TgmS35* results in disruption of the activity of respiratory complex IV, which contains the
460   mitochondrially encoded subunits (CoxI and CoxIII), at 48 hours after gene depletion
461   (Figure 5A). On the other hand, complex V, for which the subunits are encoded in the
462   nuclear genome, shows no decrease in activity at the 48-hour time point (Figure 5A).
463   Complex V only shows a defect after a long period of *TgmS35* depletion, potentially due
464   to secondary effects (Figure 5B). We further show that the assembly and activity of the
465   TOM complex is unaffected at the 96-hour time point (Figure 5C). This approach of
466   comparing the activities of complexes that do and do-not depend on mitochondrial
467   translation for their assembly and activity provides a measure of mitochondrial
468   translation in Apicomplexa and can be used in future studies to assess the involvement
469   of other candidates with putative roles in mitochondrial translation, as well as the impact
470   of drugs aimed at mitochondrial translation inhibition. Apicomplexan ribosomal proteins
471   are not well studied. To our knowledge this is the first functional characterisation of a
472   mitochondrial ribosomal protein in *T. gondii*. Our observations point to mitochondrial
473   translational defect upon *TgmS35* depletion, thus supporting the role of *Tg*mS35 in the
474   translation machinery. Finally, the data provides additional support to an active
475   mitochondrial translation in these parasites.

476

477   In model organisms, *in vitro* functional assays performed with isolated mitochondria are
478   extensively used to unravel mitochondrial functions including translation. Previously
479   functional analysis of apicomplexan mitochondria has been hampered by the lack of
480   good quality, large-scale, organelle enrichment protocols. This led to a reliance on whole
481   cell biochemistry (e.g. Ke et al., 2018; Seidi et al., 2018) and on fluorescence
482   microscopy analysis using fluorescent dyes (e.g. Vercesi et al., 1998; Garbuz and
483   Arrizabalaga, 2017; Ovciarikova et al., 2017) for mitochondrial functional studies. Here,
484   we developed an organelle enrichment protocol which generates high quantity fractions
485   enriched with active mitochondria that can be used to investigate the activity of
486   mitochondrial pathways *in vitro*. For example, enriched mitochondria are used for the

12

487 complex V enzymatic activity performed using native-PAGE technique (Figure 5B and
488 (Salunke et al., 2018)). The protocol we develop here for one of the most tractable
489 apicomplexan parasites can be used to develop additional assays. By this, our work
490 provides an avenue for prioritising mechanistic studies of these key conserved proteins.
491 We found that the use of nitrogen cavitation to lyse *T. gondii* tachyzoites results in
492 optimal lysis (Table S4), while maintaining any of the macromolecular-complexes
493 examined here intact (TOM, complex IV, complex V and the putative mitochondrial small
494 ribosome subunit (Figures 4B, 5B, C)). Nitrogen cavitation has previously been used for
495 mitochondrial enrichment in *Plasmodium* (Mather et al., 2010; Kobayashi et al., 2007;
496 Hata et al., 2018) and in the unrelated single cell eukaryote Trypanosomes (Schneider et
497 al., 2007). We envisage this protocol will be invaluable for future efforts in the field to
498 study *Toxoplasma* mitochondrial biochemistry, and to characterise other *Toxoplasma*
499 organelles.
500
501
502

13

503   **Material and methods**

504

505   ***In silico* mining**

506

507   The mRNA abundance dataset generated by (Behnke et al., 2010) was queries via
508   GeneSpring 11.0. Of the 14 homologs of mitochondrial protein import components
509   (Table 1) 3 do not have cyclical expression pattern (Table S1.1). For each of the
510   remaining 11, we searched for other genes with correlating cyclical expression patterns.
511   We run Euclid and Spearman correlation tests at 0.9 and 0.95 scores and kept lists of
512   correlation that were smaller than 70. This search identified 281 non-overlapping genes
513   (the original search was performed with release 7.2 of ToxoDB, TGME49 strain; the
514   same group of genes now correspond to 279 predicted genes from this strain)(search
515   steps are shown in Table S1.2).
516   The orthology search leading to the 43 gene list was performed via the ToxoDB link to
517   OrthoMCL. A search strategy queried for *Toxoplasma* genes with orthologs in
518   *Plasmodium* 3D7 and with no orthologs in the three *Cryptosporidium* spp genomes
519   available. The group of TGME49 genes that comply with these criteria was intersected
520   with the 279 group resulting in 43 genes (Table S1.2, column C). Likewise, sorting based
521   on fitness phenotypes scores was performed via the ToxoDB tool. All TGME49 genes
522   were converted to their TGGT1 syntenic orthologs and then sorted according to their
523   fitness scores.
524   The probability of export to the mitochondria was assessed using the MitoProt II
525   algorithm (v.1.101) (Claros and Vincens., 1996) (https://ihg.gsf.de/ihg/mitoprot.html).
526   Candidates with a MitoProt II score above 0.9 were considered to have a high probability
527   of mitochondrial targeting, between 0.5-0.9 a medium probability, and below 0.5 a low
528   probability. Export of mitochondria was also assessed using Predotar algorithm (v.1.04)
529   (Small et al., 2004) (https://urgi.versailles.inra.fr/predotar/) with the "possibility of plastid
530   targeting" option selected.

531

532   **Plasmid construct**

533

534   For ligation independent cloning (LIC), between 500pb to 1.5kb homologous region of
535   the 3' end of each GOI was amplified by PCR from *T. gondii* RH genomic DNA with LIC
536   sequence flanking these regions (primers are in Table S2). Products were LIC-cloned
537   into linearised p3HA.LIC.CATΔpac containing a triple HA epitope tag as described
538   previously (Huynh and Carruthers, 2009; Sheiner et al., 2011). The vectors were
539   transfected into the TATiΔku80 line (Sheiner et al., 2011) and selected with
540   chloramphenicol.
541   For expression of tagged minigenes, the corresponding cDNAs were cloned (primers in
542   Table S2) into the pDT7S4 expression vector that fuses a C-terminal Myc eptitope tag
543   (van Dooren et al., 2008) via BglII and AvrII restriction sites, or into pTUB8mitoYFPFRB-
544   DHFR vector that fuses a C-terminal YFP (Jimenez and Meissner unpublished, kind gift
545   from Markus Meissner) via BstBI and NcoI restriction sites.

546 For promoter replacement, the ChopChoP (http://chopchop.cbu.uib.no/) tool was used to
547 identify gRNAs covering the ATG of each GOI. The corresponding gRNAs were cloned
548 into a U6 promoter and CAS9-GFP expressing vector (Tub-Cas9-YFP-pU6-ccdB-
549 tracrRNA) (Curt et al., 2015) using the BsaI restriction site, and the final plasmid was
550 purified by DNA midi-prep (Qiagen) per the manufacturer's protocol. The DHFR
551 selectable cassette and ATc repressible promoter were amplified by PCR from
552 pDT7S4myc (van Dooren et al., 2008; Sheiner et al., 2011). Parasites were transfected
553 with 50ug of the gRNA/CAS9 vector-PCR product mixture, and cassette integration was
554 selected with pyrimethamine.
555 For transient gene disruption, each gene specific gRNA (sequences in Table S2) vector,
556 synthesised by GenScript using backbone vector pU6-SAG1gRNA-DHFR (Serpeloni et
557 al., 2016), was co-transfected with the CAS9-FLAG expressing vector (pU6-universal)
558 (Sidik et al., 2016).
559
560 **Parasites culture**
561
562 All *T. gondii* lines were cultured on Human Foreskin Fibroblast (HFFs) in DMEM media
563 complemented with 10% FBS, 2% L-glutamine and 1% Penicillin/Streptomycin
564 antibiotics and grown at 37°C with 5 % CO_2 air atmosphere.
565
566 **Stable transfection**
567
568 Linearised vectors were transfected into TATiΔku80 (Sheiner et al., 2011) expressing
569 line by electroporation. Parasites were selected by adding the appropriate drug to the
570 culture medium for up to 2 weeks, then cloned on 96 well plates. Positive clones were
571 screened by PCR using the appropriate primers listed in Table S2.
572
573 **Immunofluorescence assay and Microscopy**
574
575 Parasites were inoculated onto human foreskin fibroblasts (HFFs) on coverslips for the
576 mentioned time period and fixed with 4% paraformaldehyde (PFA) for 20 minutes at
577 room temperature (RT). The PFA was washed away thrice with phosphate buffer saline
578 (PBS). Cells were then permeabilised and blocked with blocking buffer (PBS, 0.2%
579 Triton X-100, 2% Bovine Serum Albumin, BSA) for 20 minutes at RT. Cells were then
580 labelled with different sets of primary and secondary antibodies: mouse anti-HA antibody
581 (1:1000, Sigma), mouse anti-FLAG (1:1000), rabbit anti-TgMys (1:000) (Ovciarikova et
582 al., 2017), mouse anti-Myc (1:1000, Cell Signalling), rabbit anti-TgTOM40 (1:2000)(van
583 Dooren et al., 2016); coupled with goat anti-mouse or anti-rabbit fluorescent antibody
584 (AlexaFluor 594 or 488 1:1,000 (Invitrogen)). Primary antibodies were incubated for 1
585 hour at RT. Coverslips were then washed thrice for 5 minutes with PBS-0.2% Triton X-
586 100 and incubated with secondary antibodies for 45 minutes at RT in the dark.
587 Coverslips were washed as above and mounted on microscope slides using DAPI-
588 fluoromountG (Southern Biotech). Images were taken using a Delta Vision microscope
589 as described (Ovciarikova et al., 2017).

Mitochondrial morphology scoring

CRISPR/Cas9 transient expression - Parasites transiently co-expressing CAS9-FLAG expressing vector (pU6-universal) (Sidik et al., 2016) and gene specific sgRNA containing vector (Serpeloni et al., 2016), for genes *TGME49_214790*/*263680* and *226280,* were fixed 24 hours post-transfection. The CAS9-FLAG and mitochondria were visualised by immunofluorescence as described above. 50 vacuoles of CAS9-FLAG expressing parasites for each gene were then counted and mitochondrial morphology was assessed as followed: mitochondrial morphologies were sorted into two categories: (a) "normal" mitochondrial morphology (open, sperm-like morphologies (Ovciarikova et al; 2017)), (b) abnormal morphology (anything other than open and sperm-like morphologies), then scored. Dead parasites (displaying one or two balled mitochondria (Ovciarikova et al; 2017)) were not considered. Experiments were performed in triplicate.
Conditional knockdown - rTgmS35-3xHA mutant line was grown in the presence or absence of ATc 0.5 μM for 48 hours, fixed and mitochondria were visualized by immunofluorescence using anti-TgMys, as described above. Mitochondrial morphology was scored in the same manner as described for the above. Experiments were performed in triplicate, and a Chi-squared statistical test was performed.

Plaque assay

1000, 300 and 100 parasites were inoculated in 6-well plates in duplicates, in the presence or absence of ATc 0.5 μM for 9 days. Cells were then fixed with 100% methanol for 5 minutes at RT, washed with PBS and crystal violet dye was added for 2 hours at RT to stain host cells, and then washed with PBS.

Western Blot

Samples were resuspended in 1X NuPAGE LDS loading dye (Invitrogen) with 5% v/v beta-mercaptoethanol, then boiled at 95°C for 5 minutes and separated by SDS-PAGE. Proteins were transferred under wet conditions to nitrocellulose membrane (0.45 μm Protran™). Blots were labelled with the appropriate set of antibodies: primary rat anti-HA (1:500, Sigma), mouse anti-Myc (1:1000, Cell signalling) or rabbit anti-TgTOM40 (1:2000, (van Dooren et al., 2016)) antibodies coupled to secondary horseradish peroxidase (HRP)(Promega for mouse and rabbit, Abcam for rat) conjugated antibodies (1:10,000) or secondary fluorescent antibodies IRDye® 800CW (1:10000, LIC-COR), and visualised using the Pierce ECL Western Blotting Substrate (Thermo Scientific) or the Odyssey LCX, respectively.
For the blue native-PAGE, proteins were transferred onto a PVDF membrane (0.45 μm, Hybond™) using wet transfer in Towbin buffer (0.025 M TRIS 0.192 M Glycine 10 % Methanol) for 60 minutes at 100 V. After transfer and immunolabelling revelation was carried out as described above with the Pierce ECL Western Blotting Substrate (Thermo Scientific).

634

Protein import assay

636

637 Parasites were transfected with the Hsp60$_L$-mDHFR-cMyc vector (van Dooren et al.,
638 2016) (kind gift from Giel van Dooren), after growth in the presence or absence of 0.5
639 µM ATc for 24 and 72 hours. Transfected parasites were collected after an additional 24
640 hours growth in their respective treatment and western blot was performed using the
641 respective parasite pellets as described above. Band intensity was measured using the
642 ImageJ software and the ratio between the mature and pre-processed band intensity
643 was calculated. A 1-way ANOVA statistical test was performed.

644

Preparation of mitochondria enriched fraction

646

647 Parasites were cultured on HFFs in T150 flasks in the presence or absence of 0.5 µM
648 ATc. Egressed parasites were collected (or, where necessary, parasites were scraped
649 and syringed, e.g. at 96 hours) and filtered through a 3 µm pore size membrane. From
650 this point on, all steps are carried out at 4°C or on ice. Parasites were centrifuged at
651 1500 x g for 15 minutes. Media was discarded and pellets were resuspended in PBS.
652 Parasites in PBS were counted on a Neubauer chamber and centrifuged at 1500 x g for
653 15 minutes. The supernatant was discarded and the pellet resuspended in lysis buffer
654 (50mM HEPES-KOH pH 7.4, 210 mM mannitol, 70 mM sucrose, 1 mM EGTA,
655 5 mM EDTA, 10 mM KCl, 1 mM DTT, 1 protease inhibitor cocktail tablet (Complete Mini,
656 EDTA-free; Roche) per 50 ml) to a concentration of 5 x 10^8 parasites mL^{-1}. Parasites
657 were transferred into a precooled nitrogen cavitation chamber and incubated at a
658 pressure of 2750psi for 15 minutes on ice. After pressure release and centrifugation at
659 1500 x g for 15 minutes, the supernatant (lysate) was kept, and the pellet, containing
660 unbroken parasites, was resuspended again at 5 x 10^8 parasites mL^{-1} in lysis buffer.
661 Repeating rounds of nitrogen cavitation were performed until >95% of parasite lysis was
662 achieved (evaluated via counting using Neubauer chamber). Pooled lysates were span
663 down at 1500 x g to remove any remaining unbroken parasites. The lysate was then
664 aliquoted to the desired amount in microcentrifuge tubes and span down at 16,000 x g
665 for 25 minutes. Supernatant discarded and pellet used immediately or stored at -80°C
666 until use.

667

Blue-Native Polyacrylamide Gel Electrophoresis

669

670 Whole parasite or previously aliquoted enriched mitochondria fraction were mixed with
671 solubilisation buffer (750 mM aminocaproic acid, 50 mM Bis-Tris–HCl pH 7.0, 0.5
672 mM EDTA, 1 % (w/v) dodecyl maltoside) and incubated on ice for 5 minutes. The
673 mixture was centrifuged at 16,000 x g at 4°C for 10 minutes. The supernatant containing
674 solubilised membrane proteins was transferred into a new microcentrifuge tube and
675 0.25% (w/v) Coomassie G250 (final concentration) was added. The anode buffer (50
676 mM Bis-Tris–HCl pH 7.0) and cathode buffer (50 mM Tricine, 15 mM Bis-Tris–HCl pH
677 7.0, 0.02% Coomassie G250 (Serva)) were poured into their respective tank

17

678 compartment and the appropriate amount of protein (55μg or 5x10^5 parasites) was
679 loaded per lane on a NativePAGE™ 4-16% Bis-Tris Gel (Novex- Life technologies). 5 μl
680 NativeMark™ (Invitrogen) was used as a molecular weight marker. Gels were run for
681 ~45 minutes at 100 V, 4-10 mA at 4°C with cathode buffer containing 0.02% (w/v)
682 Coomassie G250, then for ~2.5 hours at 250 V, 15 mA with cathode buffer containing
683 0.002% (w/v) Coomassie G250, until the dye front reached the bottom of the gel.
684
685 **High resolution Clear-Native Polyacrylamide Gel Electrophoresis**
686
687 Carried out as described in (Wittig et al., 2007) with minor modifications. Briefly, Whole
688 parasite or previously aliquoted mitochondria enriched fraction (75 μg) were mixed with
689 solubilisation buffer (50 mM NaCl, 50 mM Imidazole, 2 mM 6-aminohexanoic acid, 1 mM
690 EDTA – HCl pH 7.0, 2% (w/v) n-dodecylmaltoside) and incubated on ice for 10 minutes.
691 The mixture was centrifuged at 16,000 × g at 4°C for 15 minutes. A final concentration of
692 6.25% glycerol and 0.125% Ponceau S was added to the solubilised membrane
693 proteins. The anode buffer is composed of 25 mM Imidazole – HCl pH to 7.0 and the
694 cathode buffer of 50 mM Tricine, 7.5 mM Imidazole, 0.02% w/v n-dodecylmaltoside,
695 0.05% sodium deoxycholate. Gels were run for 30 minutes at 100 V, 10 mA, then 250-
696 300 V, 15 mA at 4°C until it the dye front reached the bottom.
697
698 **In-gel activity staining**
699
700 Activity stains were carried out as described previously (Sabar et al., 2005). Briefly, gels
701 were equilibrated in buffer without staining reagents for 10 minutes. For complex IV,
702 oxidation activity was shown using 50 mM KH_2PO_4, pH 7.2, 1 mg mL^{-1} cytochrome *c*,
703 0.1% (w/v) 3,3'-diaminobenzidine tetrahydrochloride. Stains were visible after 30
704 minutes. Staining was continued with pictures taken of the stained gels at regular
705 intervals. For complex V, ATP hydrolysis activity was visualised using 35 mM Tris, 270
706 mM glycine, pH 8.4, 14 mM $MgCl_2$, 11 mM ATP, 0.3% (w/v) $Pb(NO_3)_2$. Stains were
707 visible after 1 hour. Pictures were taken against a black background for optimal
708 visualisation of white lead precipitates.
709
710 **Mass spectrometry**
711
712 Proteins were identified using nanoflow HPLC electrospray tandem mass spectrometry
713 (nLC-ESI.MS/MS) at Glasgow Polyomics. Tryptic peptides, generated using in-gel digest
714 procedure (Williams et al., 2018), were analysed as previously described (Akpunarlieva
715 et al., 2017). Protein identities were assigned using the Mascot search engine (v2.6.2,
716 Matrix Science) to interrogate protein sequences in the *T. gondii* genome sequence
717 dataset, ToxoDB 35 release. During result analysis, only peptides with Mascot score of
718 20 and above (namely the probability that this match might be a random event is 10^{-2} or
719 lower) were included in the analysis.
720
721

Acknowledgements

Author contributions

L.S. conceived the research; L.S. A.L. and A.M developed the method; A.L. A.M J.O. J.T. and L.S. performed the experiments; L.S. A.L. and A.M. discussed the data and wrote the paper.

References

Akpunarlieva, S., Weidt, S., Lamasudin, D., Naula, C., Henderson, D., Barrett, M., *et al.* (2017) Integration of proteomics and metabolomics to elucidate metabolic adaptation in *Leishmania*. *J Proteomics* **155**: 85–98.

Barbrook, A.C., Howe, C.J., Kurniawan, D.P., and Tarr, S.J. (2010) Organization and expression of organellar genomes. *Philos Trans R Soc B Biol Sci* **365**: 785–797.

Behnke, M.S., Wootton, J.C., Lehmann, M.M., Radke, J.B., Lucas, O., Nawas, J., *et al.* (2010) Coordinated progression through two subtranscriptomes underlies the tachyzoite cycle of *Toxoplasma gondii*. *PLoS One* **5**.

Bushell, E., Gomes, A.R., Sanderson, T., Anar, B., Girling, G., Herd, C., *et al.* (2017) Functional Profiling of a Plasmodium Genome Reveals an Abundance of Essential Genes. *Cell* **170**: 260–272.e8.

Charvat, R.A., and Arrizabalaga, G. (2016) Oxidative stress generated during monensin treatment contributes to altered *Toxoplasma gondii* mitochondrial function. *Sci Rep* **6**: 1–17.

Cinar, H.N., Gopinath, G., Jarvis, K., and Murphy, H.R. (2015) The complete mitochondrial genome of the foodborne parasitic pathogen *Cyclospora cayetanensis*. *PLoS One* **10**: 1–9.

Claros, M.G., and Vincens, P. (1996) Computational method to predict mitochondrially imported proteins and their targeting sequences. *Eur J Biochem* **241**: 779–786.

Curt-Varesano, A., Braun, L., Ranquet, C., Hakimi, M.A., and Bougdour, A. (2016) The aspartyl protease TgASP5 mediates the export of the *Toxoplasma* GRA16 and GRA24 effectors into host cells. *Cell Microbiol* **18**: 151–167.

Desai, N., Brown, A., Amunts, A., and Ramakrishnan, V. (2017) The structure of the yeast mitochondrial ribosome. *Science* **355**: 528–531.

Dooren, G.G. Van, Stimmler, L.M., and McFadden, G.I. (2006) Metabolic maps and functions of the *Plasmodium* mitochondrion. *FEMS Microbiol Rev* **30**: 596–630. .

Dooren, G.G. van, Tomova, C., Agrawal, S., Humbel, B.M., and Striepen, B. (2008) *Toxoplasma gondii* Tic20 is essential for apicoplast protein import. *Proc Natl Acad Sci U S A* **105**: 13574–13579.

Dooren, G.G. Van, Yeoh, L.M., Striepen, B., and McFadden, G.I. (2016) The import of proteins into the mitochondrion of *Toxoplasma gondii* . *J Biol Chem* **291**: 19335–19350.

784

785 Esseiva, A.C., Naguleswaran, A., Hemphill, A., and Schneider, A. (2004) Mitochondrial
786 tRNA import in *Toxoplasma gondii* . *J Biol Chem* **279**: 42363–42368.

787

788 Feagin, J.E. (1992) The 6-kb element of *Plasmodium falciparum* encodes mitochondrial
789 cytochrome genes. *Mol Biochem Parasitol* **52**: 145–148.

790

791 Feagin, J.E., Harrell, M.I., Lee, J.C., Coe, K.J., Sands, B.H., Cannone, J.J., *et al.* (2012)
792 The Fragmented Mitochondrial Ribosomal RNAs of *Plasmodium falciparum*. *PLoS One*
793 **7**: e38320.

794

795 Garbuz, T., and Arrizabalaga, G. (2017) Lack of mitochondrial MutS homolog 1 in
796 *Toxoplasma gondii* disrupts maintenance and fidelity of mitochondrial DNA and reveals
797 metabolic plasticity. *PLoS One* **12**: 1–23.

798

799 Goodman, C.D., Siregar, J.E., Mollard, V., Vega-rodríguez, J., Syafruddin, D., Matsuoka,
800 H., *et al.* (2016) Parasites resistant to the antimalarial atovaquone fail to transmit by
801 mosquitoes. *Science (80-)* **352**: 349–353.

802

803 Greber, B.J., and Ban, N. (2016) Structure and Function of the Mitochondrial Ribosome.
804 *Annu Rev Biochem* **85**: 103–132.

805

806 Gupta, A., Shah, P., Haider, A., Gupta, K., Siddiqi, M.I., Ralph, S.A., and Habib, S.
807 (2014) Reduced ribosomes of the apicoplast and mitochondrion of *Plasmodium* spp. and
808 predicted interactions with antibiotics. *Open Biol* **4**.

809

810 Gupta, K., Gupta, A., and Habib, S. (2018a) Characterization of a *Plasmodium*
811 *falciparum* rRNA methyltransferase. *Mol Biochem Parasitol* **223**: 13–18.

812

813 Gupta, K., Gupta, A., Haider, A., and Habib, S. (2018b) Characterization of
814 mitochondrion-targeted GTPases in *Plasmodium falciparum*. *Parasitology* **145**: 1600–
815 1612.

816

817 Hata, M., Sato, S., and Kita, K. (2018) Method for the separation of mitochondria and
818 apicoplast from the malaria parasite *Plasmodium falciparum*. *Parasitol Int* **69**: 99–102.

819

820 Hikosaka, K., Kita, K., and Tanabe, K. (2013) Diversity of mitochondrial genome
821 structure in the phylum Apicomplexa. *Mol Biochem Parasitol* **188**: 26–33.

822

823 Hillebrand, A., Matz, J.M., Almendinger, M., Müller, K., Matuschewski, K., and Schmitz-
824 Linneweber, C. (2018) Identification of clustered organellar short (cos) RNAs and of a
825 conserved family of organellar RNA-binding proteins, the heptatricopeptide repeat
826 proteins, in the malaria parasite. *Nucleic Acids Res* **46**: 10417–10431.

827

828   Huet, D., Rajendran, E., Dooren, G.G. Van, and Lourido, S. (2018) Identification of
829   cryptic stator subunits from an apicomplexan ATP synthase. *Elife* 1–22.
830
831   Huynh, M.-H., and Carruthers, V.B. (2016) Plasmodium GAMA Contributes to Parasite
832   Attachment and Cell Invasion. *mSphere* **1**: 1–15.
833
834   Huynh, M.H., and Carruthers, V.B. (2009) Tagging of endogenous genes in a
835   *Toxoplasma gondii* strain lacking Ku80. *Eukaryot Cell* **8**: 530–539.
836
837   Karnkowska, A., and Hampl, V. (2016) The curious case of vanishing mitochondria.
838   *Microb Cell* **3**: 491–494.
839
840   Karnkowska, A., Vacek, V., Zubáčová, Z., Treitli, S.C., Petrželková, R., Eme, L., *et al.*
841   (2016) A eukaryote without a mitochondrial organelle. *Curr Biol* **26**: 1274–1284.
842
843   Ke, H., Dass, S., Morrisey, J.M., Mather, M.W., and Vaidya, A.B. (2018) The
844   mitochondrial ribosomal protein L13 is critical for the structural and functional integrity of
845   the mitochondrion in *Plasmodium falciparum*. *J Biol Chem* **293**: 8128–8137.
846
847   Klug, D., Mair, G.R., Frischknecht, F., and Douglas, R.G. (2016) A small mitochondrial
848   protein present in myzozoans is essential for malaria transmission. *Open Biol* **6**.
849
850   Kobayashi, T., Sato, S., Takamiya, S., Komaki-Yasuda, K., Yano, K., Hirata, A., *et al.*
851   (2007) Mitochondria and apicoplast of *Plasmodium falciparum*: Behaviour on subcellular
852   fractionation and the implication. *Mitochondrion* **7**: 125–132.
853
854   Lin, R.Q., Qiu, L.L., Liu, G.H., Wu, X.Y., Weng, Y.B., Xie, W.Q., *et al.* (2011)
855   Characterization of the complete mitochondrial genomes of five *Eimeria* species from
856   domestic chickens. *Gene* **480**: 28–33
857   .
858   Mallo, N., Fellows, J., Johnson, C., and Sheiner, L. (2018) Protein import into the
859   endosymbiotic organelles of apicomplexan parasites. *Genes (Basel)* **9**.
860
861   Mather, M.W., Morrisey, J.M., and Vaidya, A.B. (2010) Hemozoin-free *Plasmodium*
862   *falciparum* mitochondria for physiological and drug susceptibility studies. *Mol Biochem*
863   *Parasitol* **174**: 150–153.
864
865   Nilsen, A., LaCrue, A.N., White, K.L., Forquer, I.P., Cross, R.M., Marfurt, J., *et al.* (2013)
866   Quinolone-3-Diarylethers: A New Class of Antimalarial Drug. *Sci Transl Med* **5**: 177ra37-
867   177ra37 .
868
869   Nishi, M., Hu, K., Murray, J.M., and Roos, D.S. (2008) Organellar dynamics during the
870   cell cycle of *Toxoplasma gondii* . *J Cell Sci* **121**: 1559–1568.
871

872 Ogedengbe, M.E., El-Sherry, S., Whale, J., and Barta, J.R. (2014) Complete
873 mitochondrial genome sequences from five Eimeria species (Apicomplexa; Coccidia;
874 Eimeriidae) infecting domestic turkeys. *Parasites and Vectors* **7**: 1–11.
875
876 Ovciarikova, J., Lemgruber, L., Stilger, K.L., Sullivan, W.J., and Sheiner, L. (2017)
877 Mitochondrial behaviour throughout the lytic cycle of *Toxoplasma gondii* . *Sci Rep* **7**: 1–
878 13
879 .
880 Painter, H.J., Morrisey, J.M., Mather, M.W., and Vaidya, A.B. (2007) Specific role of
881 mitochondrial electron transport in blood-stage *Plasmodium falciparum*. *Nature* **446**: 88–
882 91.
883
884 Panigrahi, A.K., Ogata, Y., Zíková, A., Anupama, A., Dalley, R.A., Acestor, N., *et al.*
885 (2009) A comprehensive analysis of *Trypanosoma brucei* mitochondrial proteome.
886 *Proteomics* **9**: 434–50
887 .
888 Phillips, M.A., Lotharius, J., Marsh, K., White, J., Dayan, A., White, K.L., *et al.* (2015) A
889 long-duration dihydroorotate dehydrogenase inhibitor (DSM265) for prevention and
890 treatment of malaria. *Sci Transl Med* **7**: 296ra111.
891 Pino, P., Aeby, E., Foth, B.J., Sheiner, L., Soldati, T., Schneider, A., and Soldati-Favre,
892 D. (2010) Mitochondrial translation in absence of local tRNA aminoacylation and
893 methionyl tRNAMet formylation in Apicomplexa. *Mol Microbiol* **76**: 706–718.
894
895 Ramrath, D.J.F., Niemann, M., Leibundgut, M., Bieri, P., Prange, C., Horn, E.K., *et al.*
896 (2018) Evolutionary shift toward protein-based architecture in trypanosomal
897 mitochondrial ribosomes. *Science (80-)* **362**.
898
899 Sabar, M., Balk, J., and Leaver, C.J. (2005) Histochemical staining and quantification of
900 plant mitochondrial respiratory chain complexes using blue-native polyacrylamide gel
901 electrophoresis. *Plant J* **44**: 893–901.
902
903 Salunke, R., Mourier, T., Banerjee, M., Pain, A., and Shanmugam, D. (2018) Highly
904 diverged novel subunit composition of apicomplexan F-type ATP synthase identified
905 from *Toxoplasma gondii* . *PLoS Biol* **16**: e2006128.
906
907 Salvato, F., Havelund, J.F., Chen, M., Rao, R.S.P., Rogowska-Wrzesinska, A., Jensen,
908 O.N., *et al.* (2014) The Potato Tuber Mitochondrial Proteome. *Plant Physiol* **164**: 637–
909 653
910 .
911 Schneider, A., Charrière, F., Pusnik, M., and Horn, E. (2007) Isolation of mitochondria
912 from procyclic *Trypanosoma brucei*. *Methods Mol Biol* **372**: 67–80.
913
914 Seeber, F., Ferguson, D.J.P., and Gross, U. (1998) Toxoplasma gondii : A
915 paraformaldehyde-insensitive diaphorase activity acts as a specific histochemical marker

916   for the single mitochondrion. *Exp Parasitol* **89**: 137–139.

917

918   Seidi, A., Muellner-Wong, L.S., Rajendran, E., Tjhin, E.T., Dagley, L.F., Aw, V.Y., *et al.*
919   (2018) Elucidating the mitochondrial proteome of *Toxoplasma gondii* reveals the
920   presence of a divergent cytochrome c oxidase. *Elife* **7**: 1–36.

921

922   Seidman, D., Johnson, D., Gerbasi, V., Golden, D., Orlando, R., and Hajduk, S. (2012)
923   Mitochondrial membrane complex that contains proteins necessary for tRNA import in
924   *Trypanosoma brucei*. *J Biol Chem* **287**: 8892–8903.

925

926   Serpeloni, M., Jiménez-Ruiz, E., Vidal, N.M., Kroeber, C., Andenmatten, N., Lemgruber,
927   L., *et al.* (2016) UAP56 is a conserved crucial component of a divergent mRNA export
928   pathway in *Toxoplasma gondii* . *Mol Microbiol* **102**: 672–689.

929

930   Sharma, A., and Sharma, A. (2015) *Plasmodium falciparum* mitochondria import tRNAs
931   along with an active phenylalanyl-tRNA synthetase. *Biochem J* **465**: 459–469.

932

933   Sheiner, L., Demerly, J.L., Poulsen, N., Beatty, W.L., Lucas, O., Behnke, M.S., *et al.*
934   (2011) A systematic screen to discover and analyze apicoplast proteins identifies a
935   conserved and essential protein import factor. *PLoS Pathog* **7**.

936

937   Sheiner, L., Vaidya, A.B., and McFadden, G.I. (2013) The metabolic roles of the
938   endosymbiotic organelles of *Toxoplasma* and *Plasmodium* spp. *Curr Opin Microbiol* **16**:
939   152–158.

940   Sidik, S.M., Hackett, C.G., Tran, F., Westwood, N.J., and Lourido, S. (2014) Efficient
941   genome engineering of *Toxoplasma gondii* using CRISPR/Cas9. *PLoS One* **9**.

942

943   Sidik, S.M., Huet, D., Ganesan, S.M., Huynh, M.H., Wang, T., Nasamu, A.S., *et al.*
944   (2016) A Genome-wide CRISPR Screen in *Toxoplasma* Identifies Essential
945   Apicomplexan Genes. *Cell* **166**: 1423–1435.e12.

946

947   Siregar, J.E., Syafruddin, D., Matsuoka, H., Kita, K., and Marzuki, S. (2008) Mutation
948   underlying resistance of *Plasmodium berghei* to atovaquone in the quinone binding
949   domain 2 (Qo2) of the cytochrome b gene. *Parasitol Int* **57**: 229–232.

950

951   Small, I., Peeters, N., Legeai, F., and Lurin, C. (2004) Predotar: A tool for rapidly
952   screening proteomes for N-terminal targeting sequences. *Proteomics* **4**: 1581–1590.

953

954   Smith, A.C., and Robinson, A.J. (2018) MitoMiner v4.0: an updated database of
955   mitochondrial localization evidence, phenotypes and diseases. *Nucleic Acids Res* 1–4.

956

957   Srivastava, I.K., Rottenberg, H., and Vaidya, A.B. (1997) Atovaquone, a Broad Spectrum
958   Antiparasitic Drug, Collapses Mitochondrial Membrane Potential in a Malarial Parasite*.
959   *J Biol Chem* **272**: 3961–3966.

960

961   Suplick, K., Akella, R., Saul, A., and Vaidya, A.B. (1988) Molecular cloning and partial
962   sequence of a 5.8 kilobase pair repetitive DNA from *Plasmodium falciparum*. **3** 289-290.
963

964   Tschopp, F., Charrière, F., and Schneider, A. (2011) In vivo study in *Trypanosoma*
965   *brucei* links mitochondrial transfer RNA import to mitochondrial protein import. *EMBO*
966   *Rep* **12**: 825–832.
967

968   Vaidya, A.B., Akella, R., and Suplick, K. (1989) Sequences similar to genes for two
969   mitochondrial proteins and portions of ribosomal RNA in tandemly arrayed 6-kilobase-
970   pair DNA of a malarial parasite. *Mol Biochem Parasitol* **35**: 97–107.
971

972   Vercesi, A.E., Rodrigues, C.O., Uyemura, S.A., Zhong, L., and Moreno, S.N.J. (1998)
973   Respiration and oxidative phosphorylation in the apicomplexan parasite *Toxoplasma*
974   *gondii* . *J Biol Chem* **273**: 31040–31047.
975

976   Williams, J.J.L., Alotaiq, N., Mullen, W., Burchmore, R., Liu, L., Baillie, G.S., *et al.* (2018)
977   Interaction of suppressor of cytokine signalling 3 with cavin-1 links SOCS3 function and
978   cavin-1 stability. *Nat Commun*.
979

980   Wittig, I., Karas, M., and Schägger, H. (2007) High Resolution Clear Native
981   Electrophoresis for In-gel Functional Assays and Fluorescence Studies of Membrane
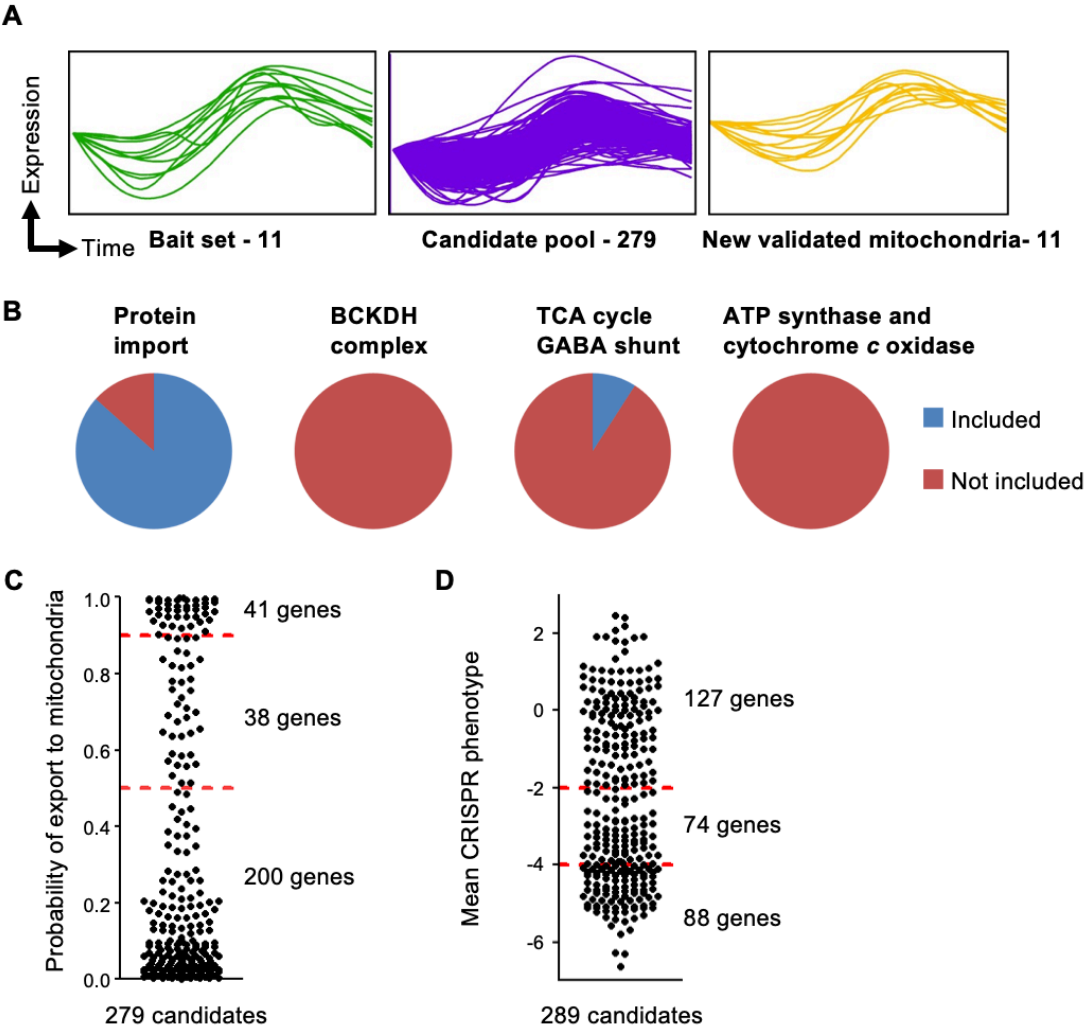982   Protein Complexes. *Mol Cell Proteomics* **6**: 1215–1225.
983

Figure 1. Discovering new mitochondrial proteins using mRNA expression data. (**A**) Graphs show mRNA abundance profiles of the bait set (left, green), candidate pool (middle, purple) and newly validated mitochondrial proteins (right, yellow) over two consecutive tachyzoite cell-cycles. (**B**) Pie charts depicting the inclusion or exclusion of genes from the candidate pool of 279 in functional groups of mitochondrial proteins (protein import, BCKDH complex, TCA cycle and GABA shunt, and ATP synthase and cytochrome *c* oxidase)(geneIDs are in Table S1.3). (**C**) Scatter plot depicting the distribution of the probability of export to the mitochondria of the 279 candidates, assessed using MitoProt II. Candidates with MitoProt score above 0.9 have a high probability of mitochondrial targeting, between 0.5-0.9 a medium probability, and below 0.5 have a low probability. (**D**) Scatter plot depicting the distribution of the mean fitness phenotype scores from the whole genome CRISPR screen of the 279 candidates (genes were first converted from *TGME49* to their orthologous and syntenic *TGGT1* gene models, giving 289 candidates). Genes with a score below -4 are considered "critical", between -2 and -4 as "important", and above -2 as "dispensable". Full datasets for each list are described in Tables S1.2.

Gene ID	Predicted product (TGME49)	Localisation Form of tagging	Phylogeny comment	MitoProt	Predotar	Proximity tagging proteome	Phenotype score
10 genes with hypothetical gene product from the 279-gene dataset							
TGME49_203620[§]	hypothetical protein	Mitochondrial cDNA	Apicomplexan unique^	0.9734	0.53	no*	-4.66
TGME49_226270	hypothetical protein	Apicoplast endogenous	NA	0.0402	0.01	no	0.23
TGME49_231150	hypothetical protein	Mitochondrial endogenous		0.9986	0.33	yes	-5.21
TGME49_240270[§]	hypothetical protein	Mitochondrial cDNA	Apicomplexan unique	0.2831	0.04	no*	-4.65
TGME49_240780	hypothetical protein	Mitochondrial endogenous	Apicomplexan unique	0.3871	0.76	no	-3.95
TGME49_247740	hypothetical protein	Mitochondrial endogenous	apicomplexan and bacteria	0.0647	0.03	no*	0.31
TGME49_257110	hypothetical protein	no signal cDNA	NA	0.6373	0.01	no	-3.21
TGME49_263680	hypothetical protein	Mitochondrial endogenous	Apicomplexan unique	0.9490	0.52	no*	-4.30
TGME49_270150	hypothetical protein	Mitochondrial endogenous	Apicomplexan unique	0.9859	0.67	yes	-4.23
TGME49_310500	hypothetical protein	no signal cDNA	NA	0.9211	0.11	no*	-4.10
5 genes with chosen from the 43-gene dataset							
TGME49_201830	ribosomal protein L37	Mitochondrial endogenous	Alveolata unique^	0.9991	0.43	no	-4.94
TGME49_226280	ribosomal protein L28, putative	Mitochondrial endogenous		0.9971	0.65	yes	-4.91
TGME49_214790[§]	glycoprotein	Mitochondrial endogenous		0.8383	0.47	yes	-3.48
TGME49_311750	mago binding protein	Cytosol cDNA	NA	0.1980	0.01	no	-0.99
TGME49_312680	60S ribosomal protein L27, putative	Mitochondrial cDNA		0.9388	0.14	no	-1.34

Table 1 – Localisation and sequence-based analysis of the 15 genes experimentally studied from the 279 candidates. Phylogenetic observations are based on search in OrthoMCL via ToxoDB and on tBLASTn via NCBI. ^OrthoMCL and BLAST search do not identify homologs outside apicomplexans or alveolates, however evidence is available for homologs outside these groups. Empty cells are where homologs are found outside apicomplexan. NA – we did not look at phylogenetic distribution when the gene product was not localised to the mitochondrion. Mitochondrial targeting predictions are done using MitoProt II (https://ihg.gsf.de/ihg/mitoprot.html) and Predotar (https://urgi.versailles.inra.fr/predotar/). The presence (yes) or absence (no) of the gene product in the proximity tagging based mitochondrial proteome is shown (Seidi et al., 2018) (no - no mass spectrometry data; no* - mass spectrometry data found but the gene is not included in the final list of 421 genes). The fitness score is based on the whole genome CRISPR/CAS9 screen (Sidik et al., 2016) (geneIDs in bold and with [§] - essentiality/importance for fitness confirmed here).
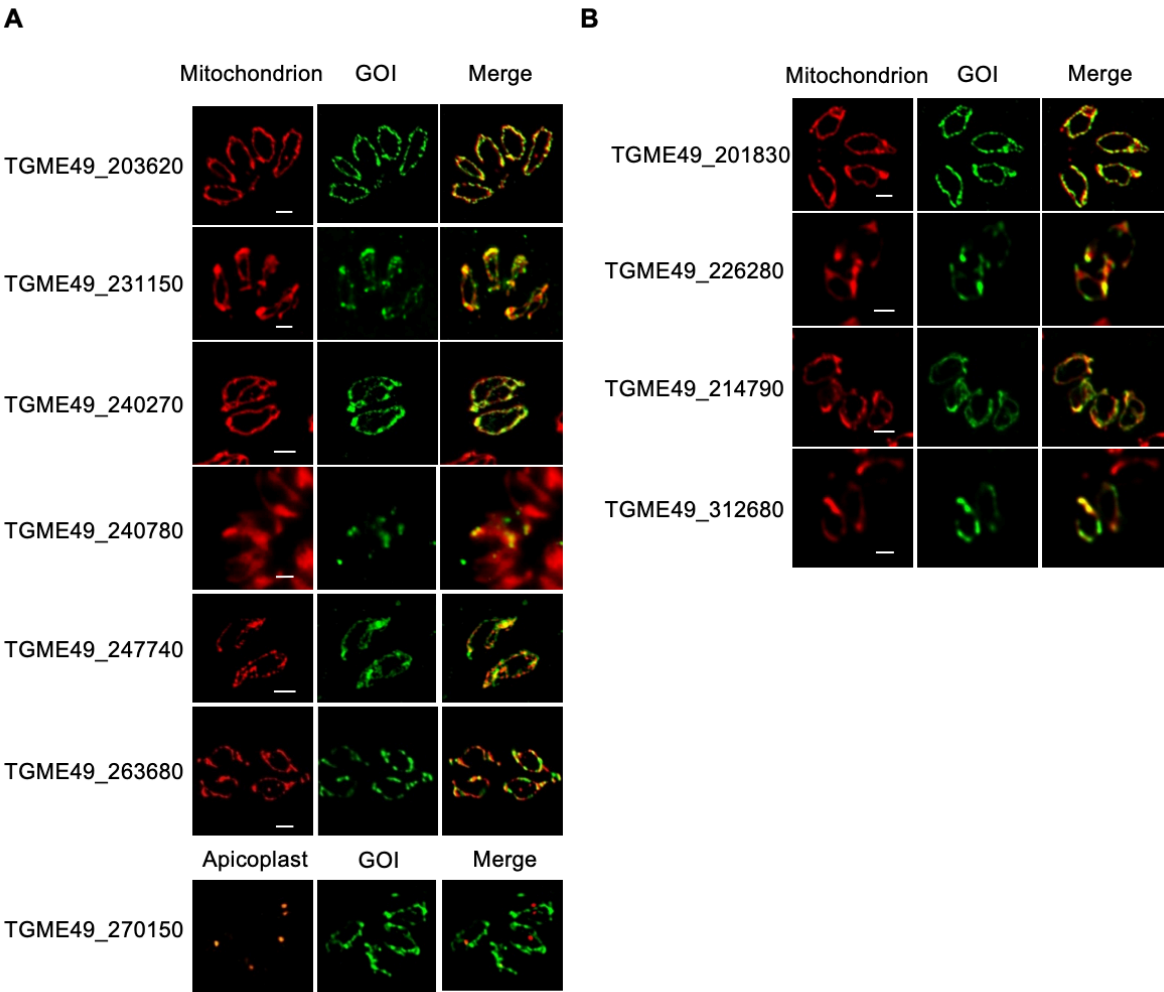
Figure 2. Mitochondrial localisation of 11 previously uncharacterised proteins by epitope tagging. (**A**) Localisation through fluorescence microscopy analysis of 7 gene-products annotated as "hypothetical proteins" from the candidate list of 279 genes. (**B**) Localisation of 4 gene-products from the candidate list of 43 genes with no homologs in *Cryptosporidium* spp. For both panels, mitochondria are marked with anti-TgMys or anti-TOM40; the mentioned GOI (gene of interest) are marked with HA or YFP; apicoplast is marked with anti-CPN60; Scale bar 1 μm.
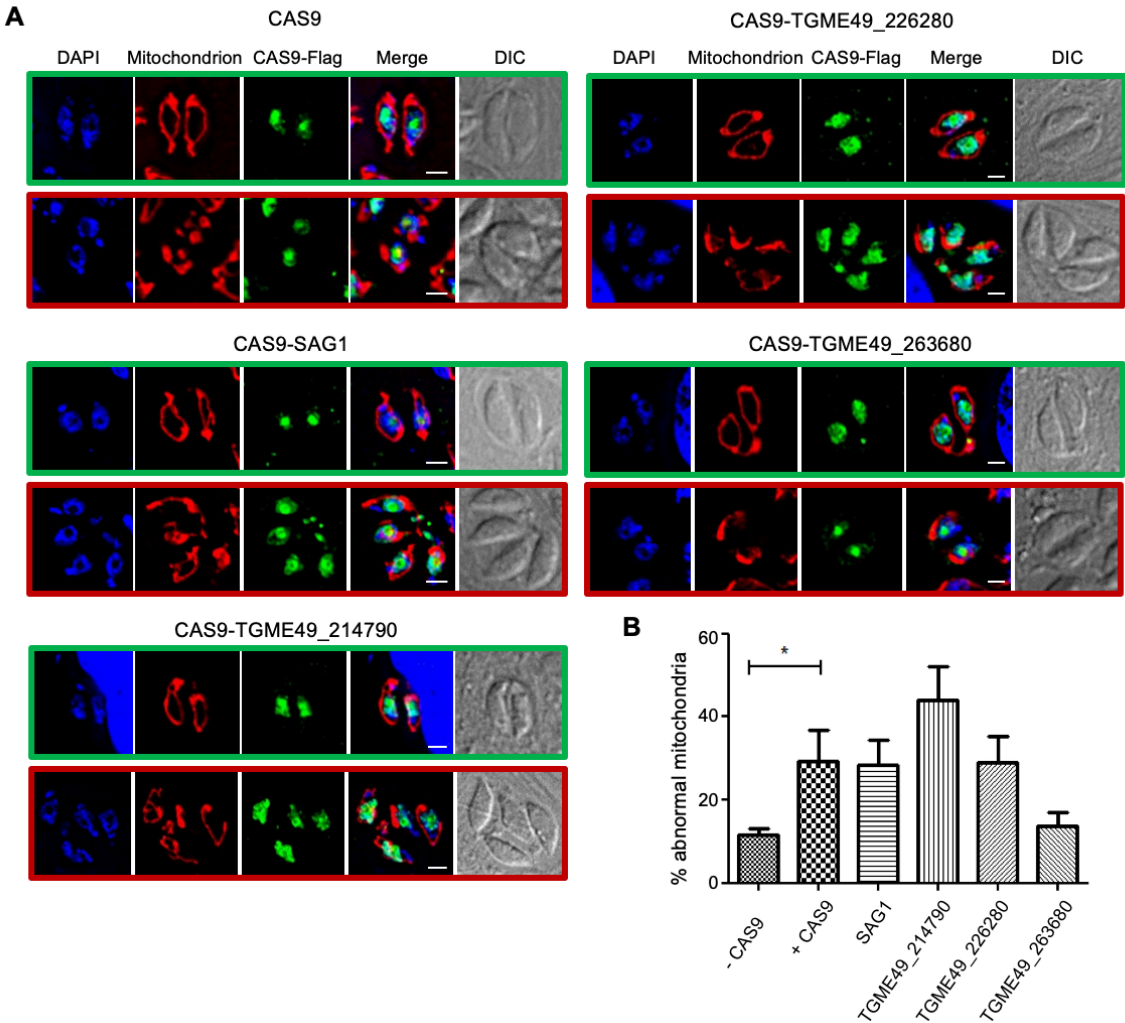
Figure 3. Transient expression of Cas9 results in mitochondria morphology defects. (**A**) Representative immunofluorescence micrographs of parasites transiently expressing CAS9 and sgRNA for the mentioned GOI. Mitochondria in red are marked by anti-TgMys. CAS9-FLAG in green is marked with anti-FLAG. Merge shows DAPI, FLAG and TgMys. Green boxes highlight parasites with wild-type looking mitochondria. Red boxes highlight parasites with mitochondria that appear to have a morphological defect herein named "abnormal mitochondria". (**B**) Quantification of vacuole with abnormal mitochondria morphologies for each condition. Bars represent the mean ± SEM (n=3), * p < 0.05 (1-way ANOVA).
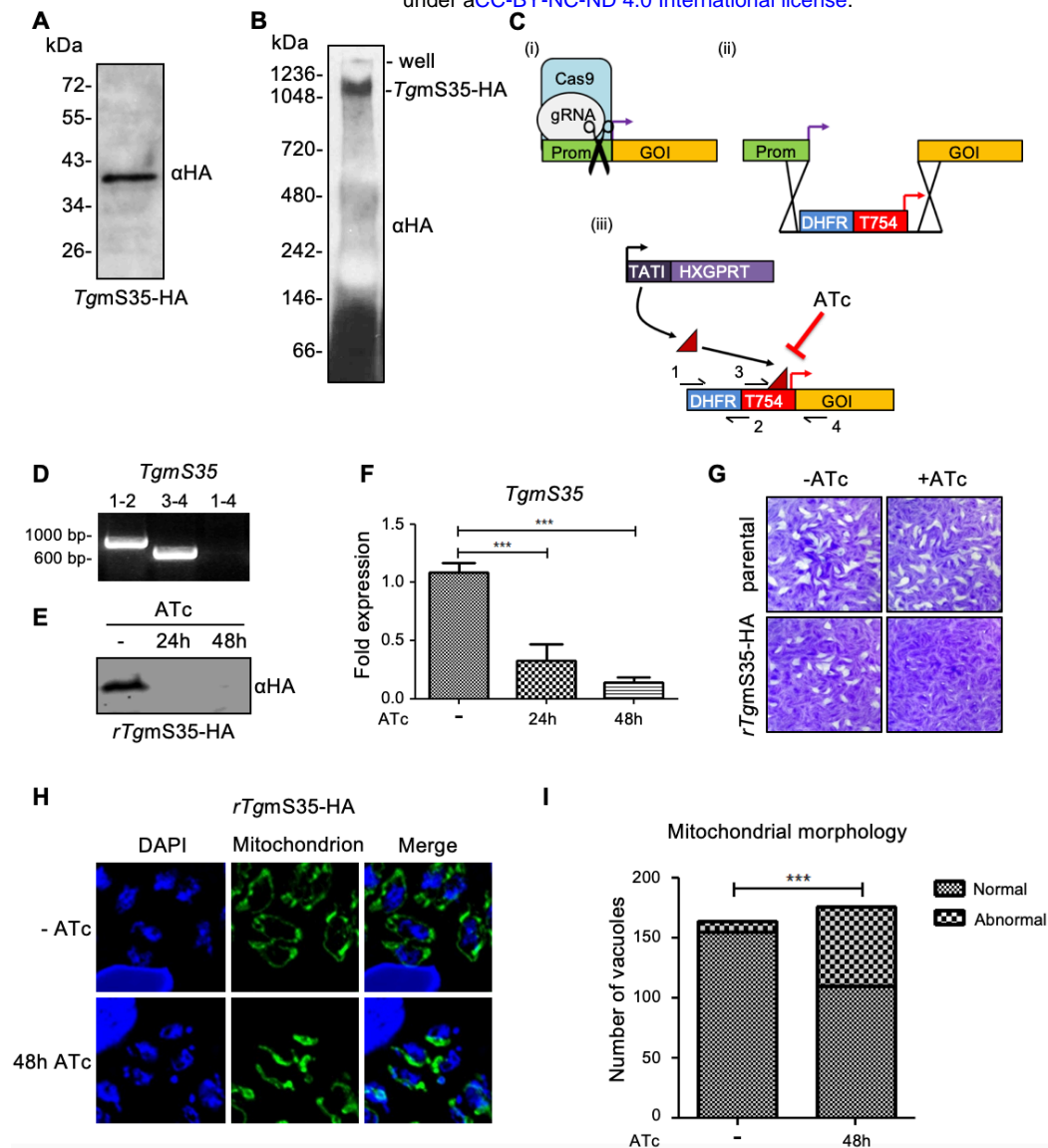
Figure 4. Knock-down and analysis of *TGME49_203620*, a homolog of the mitoribosomal subunit *mS35*. (**A**) Protein immunoblot analysis of endogenously 3xHA tagged *TgmS35* (TGME49_203620) from total cell lysate separated by SDS-PAGE and detected using an anti-HA antibody. (**B**) Total cell lysate separated by blue-native PAGE and immunoblotted to detect *Tg*mS35-3xHA with an HA antibody. (**C**) Schematic depiction of the promoter replacement strategy allowing knock-down of a GOI with the addition of ATc. (i) CRISPR/CAS9 guided cut at the predicted promoter/ATG boundary, (ii) a repair cassette containing the ATc repressible promoter, the DHFR selection marker, and homology to the promoter/ATG boundary, is inserted between the promoter and GOI, (iii) GOI, under the control of ATc repressible promoter, is down regulated when ATc is added. The black arrows represent the four primers used to confirm integration. (**D**) Validation of the promoter integration in the *Tg*mS35 locus via PCR analysis using primers 1, 2, 3, and 4, represented in C (iii). (**E**) Protein immunoblot analysis of whole cell lysate from r*Tg*mS35-HA after growth in absence (-) or presence of ATc for 24 and 48 hours. (**F**) Transcript levels of *Tg*mS35, analysed by qRT-PCR, in absence (-) or presence of ATc after 24 and 48 hours. Bars represent the mean ± SEM (n=5). ***$p < 0.0001$ (**G**) Plaque assays performed with parental line or r*Tg*mS35-3xHA parasites grown for 9 days in the absence (-) or presence (+) of ATc. (**H**) Immunofluorescence micrographs taken in the presence or absence (-) of ATc for 48h, showing examples for wild type (-ATc) or abnormal (48h ATc) mitochondrial morphologies. (**I**) Quantification of normal vs abnormal mitochondria containing vacuoles after growth of r*Tg*mS35 without (-) or with ATc for 48 hours (n=3); ***$p < 0.0001$ (Chi-squared test).
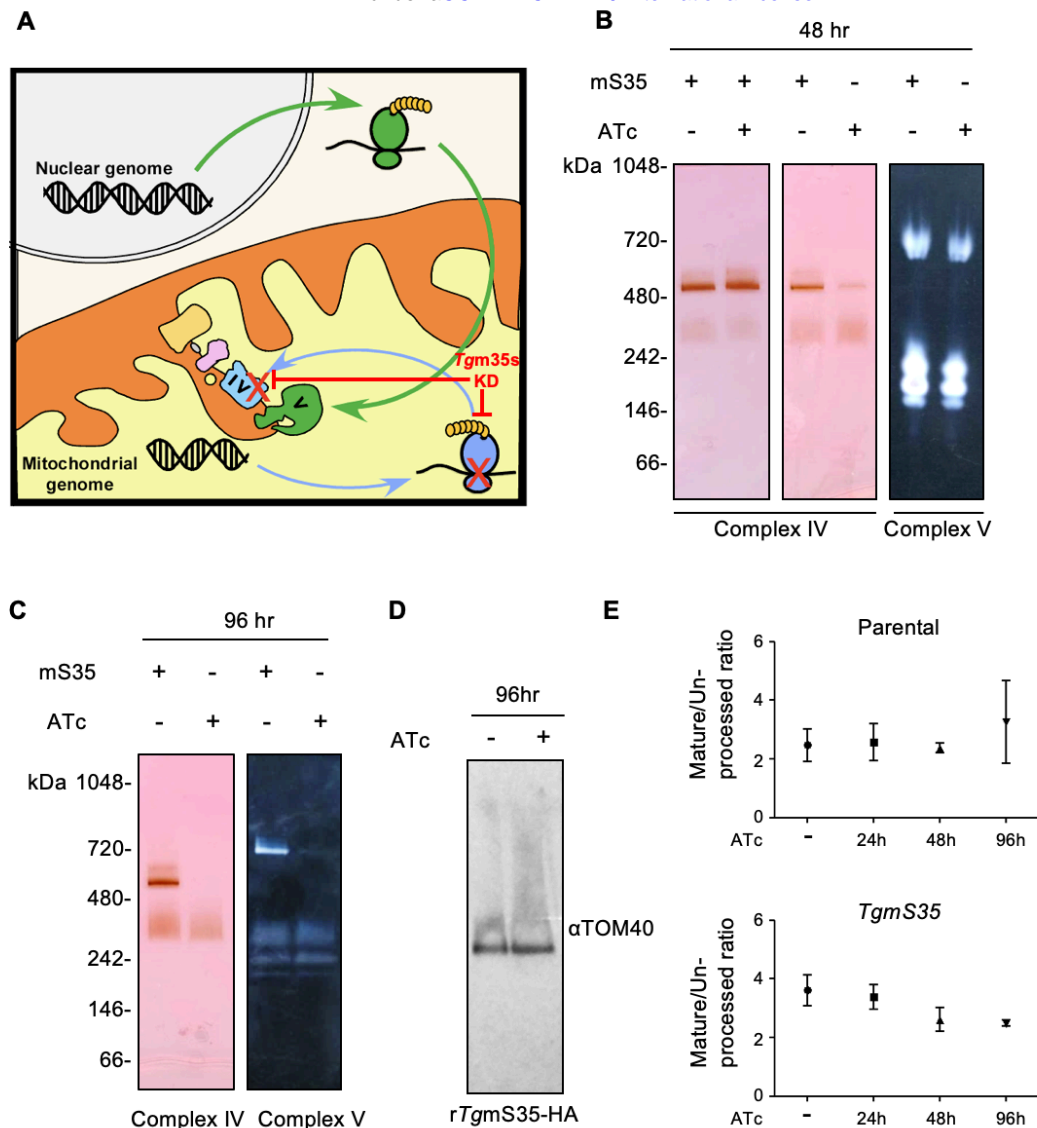
Figure 5. Down-regulation of *Tg*mS35 leads to a defect in respiratory complex IV. (**A**) A scheme describing the rational of our assay. Nuclear (grey) encoded proteins translated by the cytosolic ribosome (green) compose complex V, while mitochondrial (yellow) encoded proteins translated by the mitochondrial ribosome (blue) are necessary to assemble complex IV. Depletion of Tgm35S (red) results in reduced activity of complex IV but not V. (**B**) Whole cell (left panel) and enriched mitochondria (middle and right panel) from *Tg*mS35-3xHA (left panel) and from r*Tg*mS35-3xHA (middle and right panel), grown in the absence (-) or presence (+) of ATc for 48 hours, separated by high resolution clear-native PAGE. Complex IV activity was visualised with cytochrome *c*: DAB staining. Complex V activity was assayed by visualising the precipitation of lead by inorganic phosphate during ATP hydrolysis. Protein immunoblot analysis using anti-TOM40 of whole-cell and enriched mitochondria sample was performed as a loading control. (**C**) Mitochondrial enriched fraction from r*Tg*mS35-3xHA grown in the absence (-) or presence (+) of ATc for 96 hours, separated by high resolution clear-native PAGE and stained with coomassie or for complex IV or complex V activity as above. (**D**) Immunoblot with anti-TOM40 antibody of mitochondrial enriched fraction from r*Tg*mS35-3xHA grown in the absence (-) or presence (+) of ATc for 96 hours, separated by blue-native PAGE. (**E**) Quantification of the ratio of bands of un-processed and mature version of Hsp60$_L$-mDHFR-cMyc measured in an import assay in parental (top graph) and r*Tg*mS35-3xHA (bottom graph) parasites lines in the absence (-) or presence of ATc for 24, 48 and 96 hours. Bars represent the mean ± SEM (n=3 for the parental line, and n=5 for r*Tg*mS35-3xHA).